Inorganic Chemistry Communications xxx (xxxx) 110383

Contents lists available at ScienceDirect

Inorganic Chemistry Communications

journal homepage: www.elsevier.com/locate/inoche

Short communication

Fabrication and spectroscopic investigation of sandwich-like ZnO:rGO:ZnO:rGO:ZnO structure by layer-by-layer approach

Thangaraj Pandiyarajan [a,*], Ramalinga Viswanathan Mangalaraja [b,*], Balasubramanian Karthikeyan [c], Arunachalam Arulraj [b], M.A. Gracia-Pinilla [d,e]

[a] Department of Sciences, Indian Institute of Information Technology, Design and Manufacturing, Kurnool, Andhra Pradesh 518007, India
[b] Faculty of Engineering and Sciences, Universidad Adolfo Ibáñez, Diagonal las Torres, 2640 Peñalolén, Santiago, Chile
[c] Department of Physics, National Institute of Technology, Tiruchirappalli 620 015, India
[d] Universidad Autónoma de Nuevo León, Facultad de Ciencias Físico-Matemáticas, Av. Universidad, Cd. Universitaria, San Nicolás de los Garza, NL, Mexico
[e] Centro de Investigación en Innovación y Desarrollo en Ingeniería y Tecnología, Universidad Autónoma de Nuevo León, PIIT, Apodaca, Nuevo León 66600, México

ARTICLE INFO

Keywords:
Layer-by-layer
Reduced graphene oxide
ZnO
Spin coating
Transmission
Photoluminescence

ABSTRACT

Transparent conducting materials (TCMs) are the heart of modern optoelectronic industries and the properties of TCMs could be improved by the introduction of 2D carbon materials. In this report, the influence of order layering on microstructural, transparency and emission characteristics of ZnO:rGO:ZnO:rGO:ZnO and rGO:ZnO:rGO:ZnO:rGO sandwich structures has been investigated. The layer-by-layer approach has been adopted for the fabrication of sandwich structured materials ZnO:rGO:ZnO:rGO:ZnO and rGO:ZnO:rGO:ZnO:rGO through the spin coating technique. The sandwich structures of ZnO and rGO exhibited hexagonal wurtzite structure of ZnO without any impurities were identified through XRD. The ordering of layer's influenced the microstructural parameters and were significantly altered. The spherical nature of the particles and the formation of the sandwich structures were confirmed by using SEM micrograph. The reduction in an optical transparency and narrowing bandgap of the ZnO upon the order of layering were identified through transmission spectra. The lower energy shift of near band edge (NBE) emission and reduction in the emission intensity with respect to pure ZnO nanostructures was observed. The present work provides a simple layer-by-layer approach to fabricating sandwich structures and improving the optical properties which have potential applications in various optoelectronic devices.

1. Introduction

Transparent conducting materials (TCMs) have attracted enormous interest in recent years across the globe due to their potential use in optoelectronic devices [1], photovoltaics [2], sensors [3], and novel display devices [4,5]. The prime requirement for the TCMs is more than 90 % of optical transparency in the visible regime and very low resistivity of 10^{-4} Ω.cm [6]. Tin-doped indium oxide (ITO) materials have been fulfilled with these prime requirements and it's been widely used in the optoelectronic industries. However, due to its brittle in nature, high production cost and future unavailability, there is an extensive demand for the search of novel materials and fabrication technologies [7,8]. The doped zinc oxide (ZnO) materials are widely used as TCMs and to improve the conductivity of ZnO, various materials have been introduced which include, doping of group III elements (Al and Ga) [9,10] silver:ZnO nanocomposites [11] and introduction of two-dimensional (2D) materials [12,13].

Among various two-dimensional (2D) structured materials, graphene has drawn significant consideration because of its extraordinary electrical conductivity (2 x10^5 $cm^2V^{-1}s^{-1}$) [14], thermal (5000 $W.m^{-1}K^{-1}$) [15], mechanical properties [16] and also exhibits high optical transmittance in the visible regime [17]. Wu et al [18] have synthesized sandwich-like graphene/ZnO (5 nm diameter) nanocomposite materials and identified that the stacking of graphene sheets could be well controlled through decoration of densely packed ZnO nanostructured particles. Li et al [19] have fabricated 3D sandwich-structured ZnO/rGO/ZnO nanocomposites using rapid thermal reduction routes. The sandwich structured materials exhibited maximum capacitance (275F g^{-1}) with anomalous rate capability and cycling stability in comparison with their parent materials. Teh et al [20] fabricated the rGO-hybridized ZnO sandwich thin films using facile elec-

* Corresponding authors.
E-mail addresses: rtpandiyarajan@gmail.com (T. Pandiyarajan), rtpandiyarajan@gmail.com (R. Viswanathan Mangalaraja).

https://doi.org/10.1016/j.inoche.2022.110383
Received 5 September 2022; Received in revised form 15 December 2022; Accepted 28 December 2022
1387-7003/

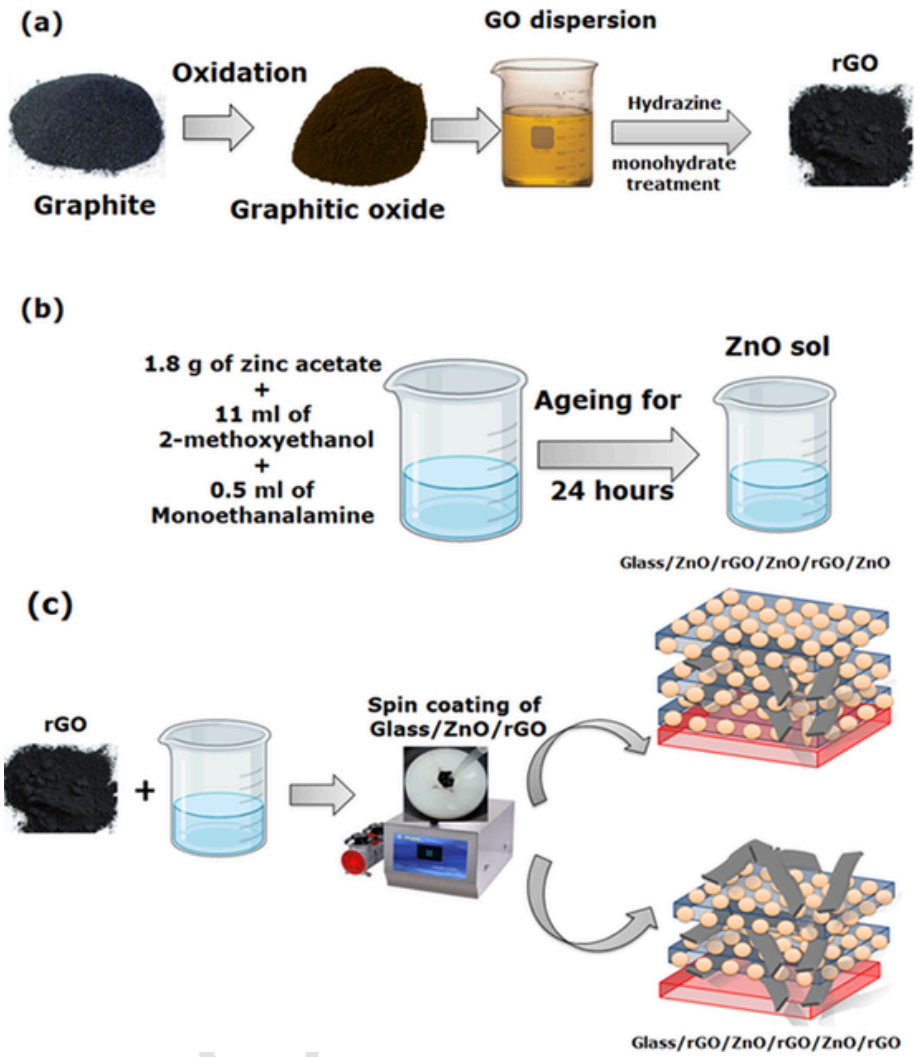

Fig. 1. Schematic representation of the synthesis of reduced graphene oxide **(a)** ZnO sol **(b)** and fabrication of ZnO:rGO:ZnO:rGO:ZnO and rGO:ZnO:rGO:ZnO:rGO sandwich structure by layer-by-layer approach **(c)**.

trodeposition route through layer-by-layer technique. Results revealed that the ordering of layer is highly influenced in the charge transfer properties which ultimately improves the efficiency of photocatalytic electrochemical water splitting. Boukhoubza et al [21] have prepared the sandwich structure of GO/ZnO nanorods/GO and evaluated their emission characteristics. The results showed that the decoration of GO layers leads quenching of PL emission intensity attributed to the charge transfer process. To date, a limited studies have been performed for the fabrication and understanding of ZnO/rGO sandwich structures and yet to be explored in details.

Considering the importance of ZnO/rGO sandwich structures in various energy and opto-electronics industries, in this report a simple layer-by-layer approach using spin coating technique has been adopted to prepare ZnO:rGO:ZnO:rGO:ZnO and rGO:ZnO:rGO:ZnO:rGO sandwich structures. The effect of layer ordering of sandwich structures on the microstructural and optical emission characteristics was investigated. Furthermore, the optical transparency of sandwich structures is analysed in a detailed manner.

2. Experimental

All the required chemicals such as zinc acetate dihydrate ($Zn(CH_3COO).2H_2O$), monoethanalamine (C_2H_7NO), are analytical grade (Sigma-Aldrich) and used as received.

2.1. Preparation of ZnO layer

In brief, 1.8 g of $Zn(CH_3COO).2H_2O$ was dissolved in 11 mL of $C_3H_8O_2$ under constant stirring followed by mixing of 0.5 mL of monoethanalamine and stirred for 60 min to get the homogeneous clear solutions. The formed sol was aged for 24 h and further used for the ZnO film preparations. The detailed procedures for the synthesis of reduced graphene oxide are reported in the supplementary section.

2.2. Fabrication of ZnO:rGO:ZnO:rGO:ZnO sandwich structure

ZnO sol solutions were deposited onto pre-cleaned glass substrates (2.5 cm × 2.5 cm) by spin coating. The rotational speed and time were kept at 2000 rpm and 30 s, respectively followed by drying at 350 °C for 10 min. The mixture of rGO powders and double distilled water are subjected to continuous sonication (42 kHz) and deposited on the ZnO film with 2000 rpm for 30 s and the procedure was repeated to achieve ZnO:rGO:ZnO:rGO:ZnO sandwich structures. To achieve a better crystalline nature, the fabricated films are calcinated at 450 °C about 1 h. The sample code is assigned according to the order of the layer deposition starting from the first layer: ZnO, rGO, ZnO:rGO, ZnO:rGO:ZnO, ZnO:rGO:ZnO:rGO, ZnO:rGO:ZnO:rGO:ZnO. For comparison, the same procedure was repeated to fabricate rGO:ZnO:rGO:ZnO:rGO sandwich

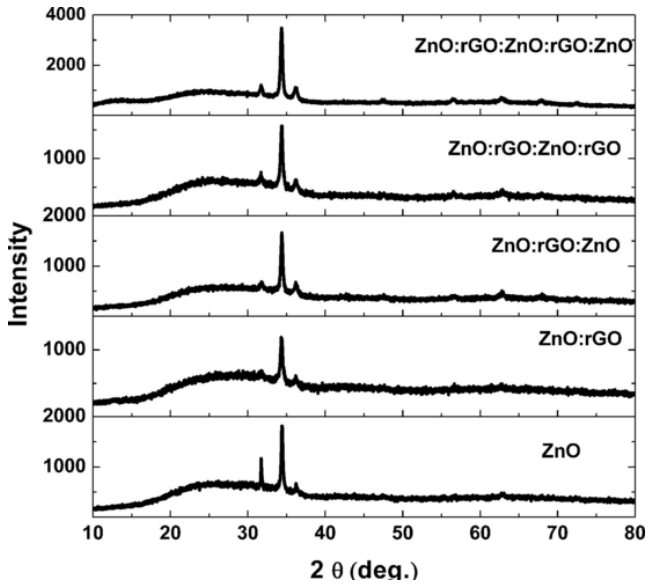

Fig. 2. XRD patterns of pure ZnO and sandwich structures of ZnO and rGO layers.

structures. Fig. 1 depicts the various process involved for the fabrication process sandwich structure.

2.3. Characterization

The phase purity, crystal structural information, and the effect of sandwich structure on orientation were analysed using powder XRD (*Bruker, D4 Endeavor*) technique with operating voltage of 40 kV and 30 mA power. The diffraction patterns are measured from (2θ) 10° to 80°. The formation of sandwich structure of prepared films was analysed using scanning electron microscope (SEM, FEI Quanta 250). The effect of sandwich structure and the layer ordering on transparency properties was studied by using UV–visible-NIR (*Shimadzu dual beam*) spectroscopy and spectra measured from 200 nm to 900 nm. The emission characteristic was identified through photoluminescence (PL) spectroscopy and was done using PerkinElmer LS 45 fluorescence spectrometer. The excitation wavelength kept at 330 nm and emission were measured from 360 nm to 600 nm.

3. Results and discussion

The XRD patterns of pure ZnO, sandwich structures of various combinations of the layer ordering of ZnO and rGO are presented in Fig. 2. The peaks located at an angle (2θ) of 31.58, 34.33, 36.26, 47.50, 56.49, 62.57, 67.86 and 72.52° are correspond to (1 0 0), (0 0 2), (1 0 1), (1 0 2), (1 1 0), (1 0 3), (1 1 2) and (0 0 4), respectively which confirmed the fabricated ZnO are in the hexagonal wurtzite structure.

There is no signature of impurities of Zn and graphite precursors identified in the recorded diffraction patterns. However, the lower angle peak (0 0 2) shift has been observed for the sandwich structure (Fig. 3b). All the samples, intensity of (0 0 2) planes are higher than the other diffraction peaks indicated that "*c*" axis is the preferential orientations. Ohyama et al have reported the (0 0 2) plane is extremely favourable orientation of the ZnO thin films which are produced from zinc acetate dihydrate as starting precursors [22].

For comparison, the fabricated pure rGO, and rGO:ZnO:rGO:ZnO:rGO sandwich structures were subjected to the XRD analysis and the corresponding obtained diffraction patterns are shown in Fig. 3a. The broad diffraction peak located at an angle (2θ) of 24.65° corresponds to the diffraction plane of rGO (0 0 2). The spacing between the layers (d_{002}) could be deducted through Bragg's equation and found to be 0.3607 nm which is slightly higher than the natural graphite samples (0.336 nm) [23]. The lattice constants of ZnO such as "*a*" axis, "*c*" axis, volume of unit cell (v) and bond length (L) could be extracted from the diffraction patterns using the formulae [24,25].

$$a = \lambda/\sqrt{3}\sin\theta \text{ for } (1\ 0\ 0) \text{ plane} \quad (1)$$

$$c = \lambda/\sin\theta \text{ for } (0\ 0\ 2) \text{ plane} \quad (2)$$

$$v = \frac{\sqrt{3}a^2c}{2} \quad (3)$$

$$L = \sqrt{\left(\frac{a^2}{3}\right) + \left(\frac{1}{2} - u_p\right)^2 c^2} \quad (4)$$

where, 'u_p' is the positional parameter which could be calculated by using the formulae

$$u_p = \frac{a^2}{3c^2} + 0.25 \quad (5)$$

The calculated lattice parameter values of the pure ZnO, ZnO:rGO:ZnO:rGO:ZnO and rGO:ZnO:rGO:ZnO:rGO sandwiched structures are listed in Table 1. From Table 1, it is observed that there is a slight change in the lattice constants of the sandwich structures. The

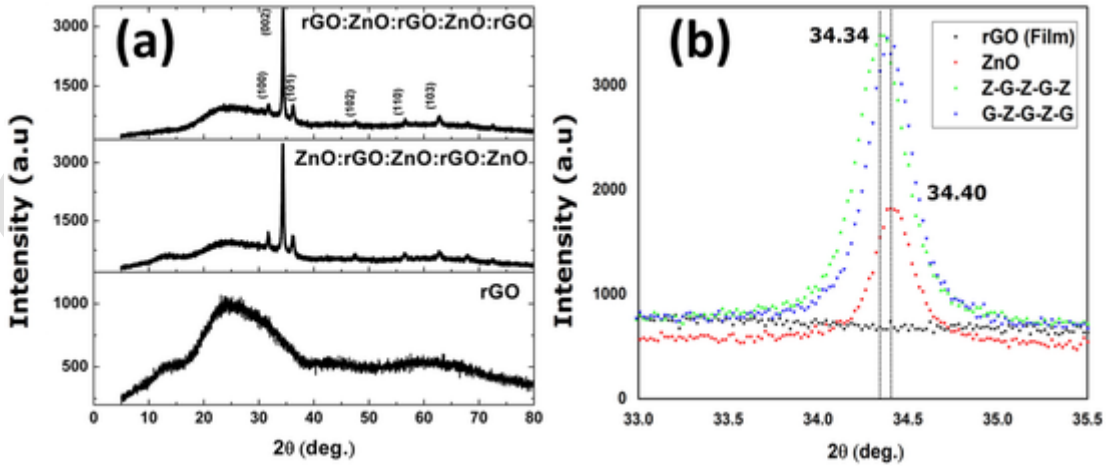

Fig. 3. (a) XRD patterns of the pure rGO, ZnO/rGO/ZnO/rGO/ZnO and rGO/ZnO/rGO/ZnO/rGO sandwich structures, and **(b)** Peak shift of (0 0 2) plane in the fabricated films.

Table 1
The calculated lattice parameters.

Sample name	*a* value (Å)	*c* value (Å)	Volume (Å)^3	Bond length (Å)	Strain (ε_z) %	Residual stress (σ)10^9
ZnO	3.2543	5.2066	47.75	1.979	0.00134	−0.0017
ZnO/rGO/ ZnO/ rGO/ZnO	3.2561	5.2166	47.89	1.982	0.19321	−0.2484
rGO/ZnO/ rGO/ ZnO/rGO	3.2513	5.2099	47.69	1.978	0.06338	−0.0815

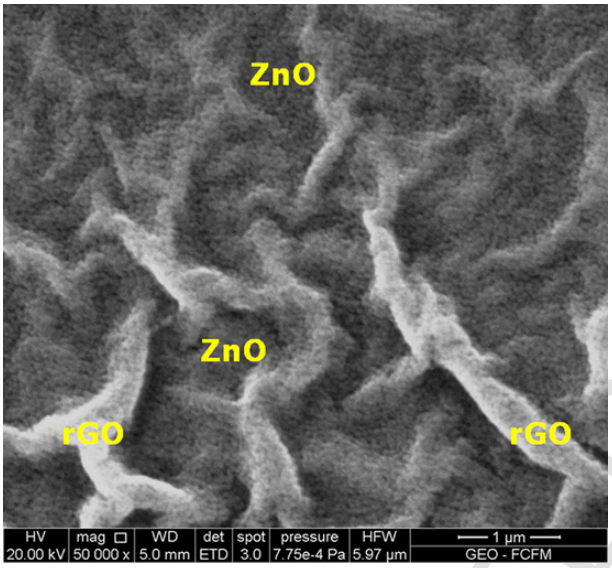

Fig. 4. SEM micrograph of ZnO/rGO/ZnO/rGO/ZnO sandwich structure.

strain produced in the films along *c*-axis could be evaluated by using the formulae [26]

$$\varepsilon_z(\%) = \left(c - c_o/c_o\right) * 100 \quad (6)$$

where c is the lattice parameter of the ZnO film and c_o is the unstrained latticed parameter of ZnO. Similarly, the residual stress could be expressed as follows

$$\sigma = \left(2c_{13}^2 - c_{33}\left(c_{11} + c_{12}\right)/2c_{13}\right) * \left(c - c_o/c_o\right) \quad (7)$$

where, c_{ij} are the elastic constants for ZnO single crystal and the values are 208.8, 213.8, 119.7 and 104.2 GPa which correspond to c_{11}, c_{33}, c_{12} and c_{13}, respectively. The estimated values of the strain and residual stress present in the samples are listed in Table 1. The positive strain value and the negative stress value confirmed that tensile strain and compressive stress were present in the materials.

The morphology and size of the ZnO nanostructures were identified using SEM micrograph and are shown in Fig. 4. It is evident that the ZnO particles are spherical in nature and the average particle size was estimated from SEM micrograph, which is found to be 55 nm. Liang et al have reported the controlled synthesis of ordered sandwich $CuCo_2O_4$/rGO composite using layer-by-layer hetero assembly for supercapacitor applications. It is observed that the single layer or ultrathin GO nanosheets are due to the formation of folds on the surface. In addition, layer-by-layer self-assembly technique makes spreads of GO nanosheets and forms a flat surface. Moreover, $CuCo_2O_4$/rGO composite *structure exhibited a decoration of uniformly sized* $CuCo_2O_4$ nanoparticles on the rGO nanosheets [27]. Teh et al [20] fabricated the rGO-hybridized ZnO sandwich thin films using a facile electrodeposition route through layer-by-layer technique. FESEM micrographs of unhybridized and rGO-hybridized ZnO thin films revealed that the ZnO thin films have vertically aligned reshapes and a diameter range between 150 nm and 1.1 µm. In addition, a thin layer of rGO has been observed in ZnO/rGO and rGO/ZnO/rGO thin films, and porous nature was observed due to the agglomeration of ZnO nano spherical particles. In the present case, rGO layer structures with folds on the surface have been observed and ZnO spherical nanoparticles are embedded in rGO structures.

The optical transmittance of the fabricated pure ZnO and the sandwich structures with various combinations of the rGO and ZnO layers are displayed in Fig. 5a. It clearly showed that the band located at 365 nm is attributed to excitonic absorption of the pure ZnO and band gets shifted to lower energy for the sandwich structures (inset of Fig. 5a). The transparency of the prepared films is presented in Fig. 5b. The obtained results revealed that pure and sandwich structured films are highly transparent at 550 nm and transparency of the pure ZnO is 85 % and it is increased to 87 % for ZnO:rGO structures. Further, the transparency of the film is reduced to 67 % at 550 nm for ZnO:rGO:ZnO:rGO:ZnO sandwich structures.

The reduction in an optical transparency and narrowing bandgap of the ZnO is mainly due to three factors: (i) the formation of ZnO-C bond, (ii) significant increase of surface charge in the presence of rGO could resulted a short electron pathway to the rGO surfaces, and (iii) the electronic coupling between the ZnO nanostrutures and rGO sheets which could lead to transfer of electrons to the rGO surfaces from the conduction band of the ZnO nanostructures. Similar kind of observation has

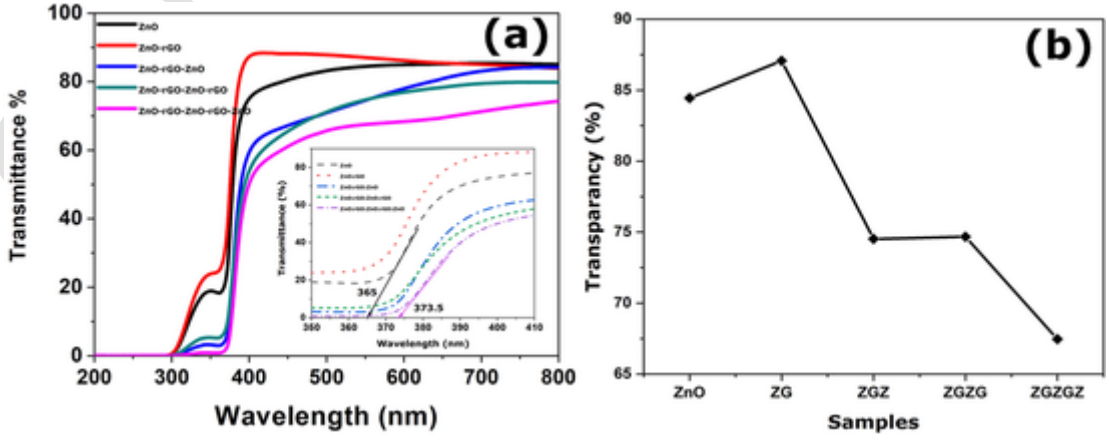

Fig. 5. (a) Transmittance spectra of pure ZnO and sandwich structures of ZnO and rGO.

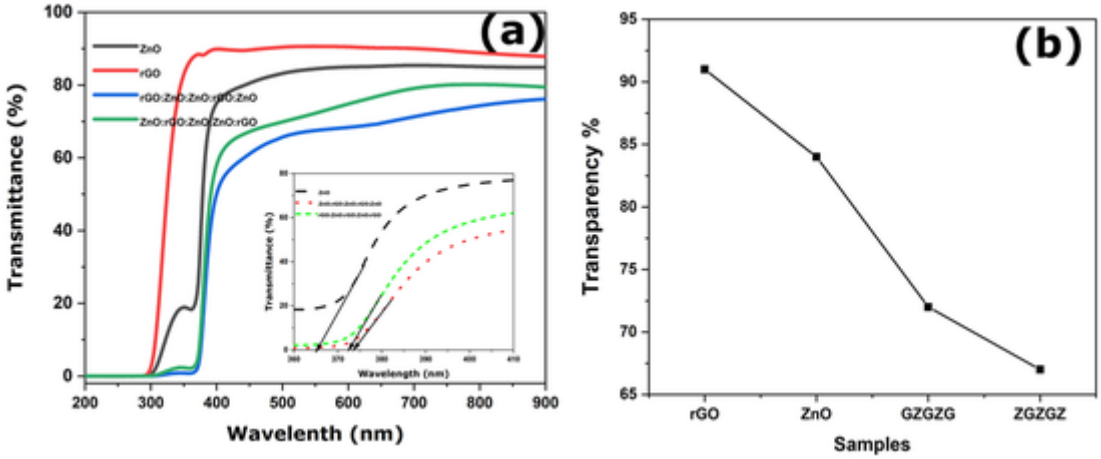

Fig. 6. (a) Transmittance spectra of pure ZnO, rGO, ZnO/rGO/ZnO/rGO/ZnO and rGO/ZnO/rGO/ZnO/rGO sandwich structures **inset (a)** enlarged view of band shift, and **(b)** represents the transparency vs various sandwich structured films.

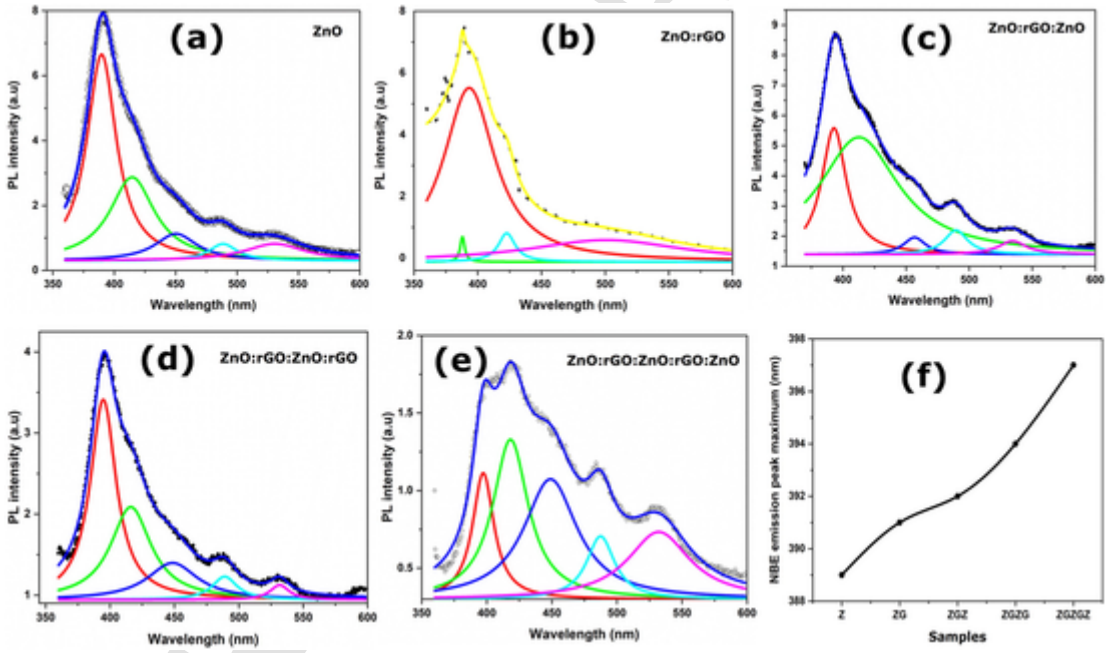

Fig. 7. (a-e) Lorentzian decomposed PL spectra of pure ZnO, sandwich structures of ZnO and rGO layers, and **(f)** Variation of NBE emission peak maximum vs samples.

been made with the ZnO/CNT composites [29], GO-ZnO composite films [30–32].

The transmittance spectra of the pure rGO, ZnO, ZnO:rGO:ZnO:rGO:ZnO and rGO:ZnO:rGO:ZnO:rGO sandwich structures are displayed in Fig. 6a. The pure rGO showed 91 % of transparency. The band shift occurred in the sandwich structures compared with pure ZnO and is displayed in inset of Fig. 6a and it reveals that the excitonic absorption band shifted to 372 nm. In addition, transparency of rGO:ZnO:rGO:ZnO:rGO sandwich structures is 72 % which slightly higher than the ZnO:rGO:ZnO:rGO:ZnO sandwich structures. The transparency vs different sandwich structured films are presented in Fig. 6b.

The Lorentzian decomposed photoluminescence spectra of the pure ZnO and various combinations of the layer ordering rGO and ZnO sandwich structures are shown in Fig. 7 (a-e). The pure ZnO films exhibited emission bands at 389, 414, 450, 488 and 530 nm. Normally, band located in the UV regime is corresponds to the NBE of ZnO and is mainly attributed to the recombination of free excitons and band between 400 and 700 nm is assigned to the visible emission. The origin of the visible emission bands in the ZnO nanostructures are mainly attributed to the various defects present in the materials. Several works have been reported for the origin of the visible emission both theoretically and experimentally [33–35]. The defect bands such neutral (V_{Zn}), singly charged (V_{Zn}^{-}), and doubly charged zinc vacancies (V_{Zn}^{2-}) are located at 3.06, 2.66 and 0.56 eV below the conduction band, respectively. The neutral zinc interstitials (Zn_i^{o} and Zn_i) and singly charged zinc interstitial (Zn_i^{+}) bands are appeared at 0.05, 0.46 and 0.5 eV, respectively. The oxygen vacancies such as neutral oxygen vacancies (V_O^{o} and V_O), and singly charged oxygen vacancy (V_O^{+}) are located at 0.05, 1.62 and 2 eV, respectively. Similarly, the oxygen interstitial (O_i) O_{Zn} and complex of an oxygen vacancy and zinc interstitial (V_oZn_i) bands are appeared at 2.96, 2.38 and 2.16 eV, respectively.

The variation of near-band-edge (NBE) emission peak maxima and sandwich structures are shown in Fig. 7f and it is evident that the decrease in the bandgap of ZnO for the sandwich layers. This is consistent with our UV transmittance results. Further, intensity of the NBE emission is decreased for both ZnO:rGO:ZnO:rGO:ZnO and

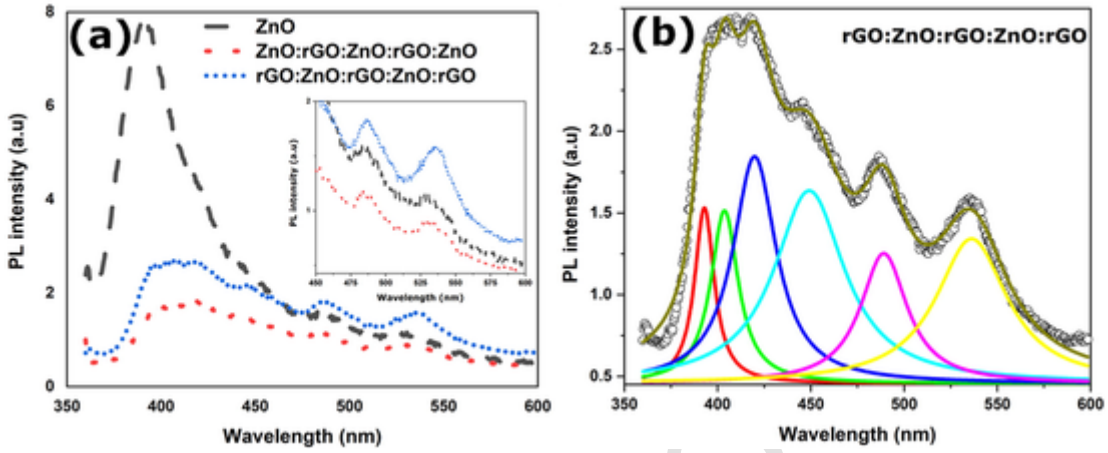

Fig. 8. (a) PL spectra of the pure ZnO, ZnO/rGO/ZnO/rGO/ZnO and rGO/ZnO/rGO/ZnO/rGO sandwich structures **inset (a)** enlarged view of visible emission bands, and **(b)** Lorentzian decomposed PL spectrum of rGO/ZnO/rGO/ZnO/rGO sandwich structures.

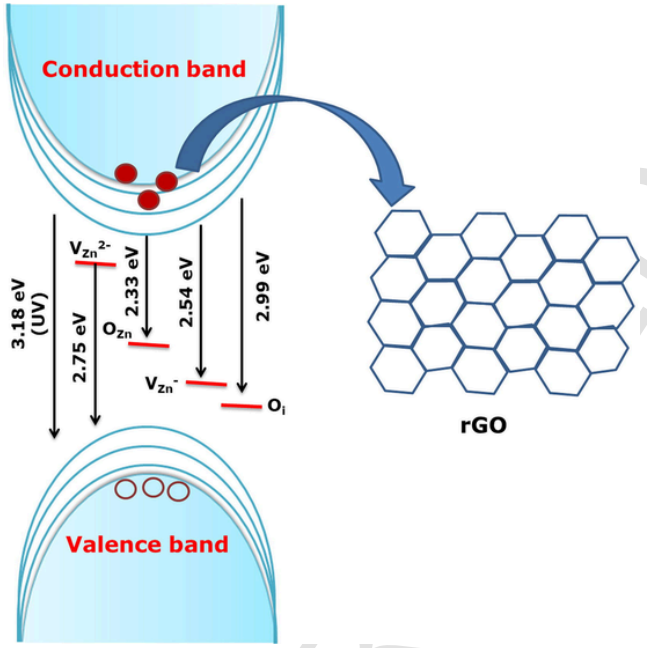

Fig. 9. A schematic diagram of the position of various defects related bands and electron transfer between the ZnO nanostructures and rGO layers.

rGO:ZnO:rGO:ZnO:rGO sandwich structures and visible band was increased for the rGO:ZnO:rGO:ZnO:rGO samples (Fig. 8a). The Lorentzian decomposed PL spectra of the rGO:ZnO:rGO:ZnO:rGO sandwich structures are presented in Fig. 8b.

The graphene sheets exhibited the 2-dimensional π-conjugation structure which could acts as very good electron-acceptor materials and thus efficiently prevent the electron-hole pair recombination process [35]. The excitation of 325 nm could enable electron transfer from the valence band to conduction band and then electron makes a transition to graphene sheets which could prevent the electron-hole recombination process. Thus, leads to reduction of emission intensity. Similar results have been observed for g-C_3N_4 composite materials [36] and Ag–ZnO-reduced graphene oxide hybrid nanostructured materials [38]. The schematic representation and the position of the various defects related bands and the effective electron transfer between the ZnO nanostructures and rGO sheets are depicted in Fig. 9.

4. Conclusion

In conclusion, ZnO:rGO:ZnO:rGO:ZnO and rGO:ZnO:rGO:ZnO:rGO sandwich structures were successfully fabricated through layer-by-layer approach using spin coating technique. The formation, various microstructural parameters, optical transparency, and emission characteristics were analysed by the different spectroscopic techniques. The unit cell volume, bond length, micro-strain and residual stress were considerable altered for the sandwich structures. The significant improvement of electronic coupling between ZnO and rGO sheets and enhancement of surface charge led to the reduction in band gap and transparency of films. The emission spectral results depicted that the NBE emission intensity was quenched and the shifted in the NBE emission caused due to the effective electron transfer. Based on the obtained results, the fabricated sandwich structures may have an immense application in the various optoelectronic devices.

Uncited reference

[28].

CRediT authorship contribution statement

Thangaraj Pandiyarajan : Conceptualization, Methodology, Investigation, Writing – original draft. **Ramalinga Viswanathan Mangalaraja :** Supervision, Writing – review & editing. **Balasubramanian Karthikeyan :** Supervision. **Arunachalam Arulraj :** Resources. **M.A. Gracia-Pinilla :** Investigation, Resources.

Declaration of Competing Interest

The authors declare that they have no known competing financial interests or personal relationships that could have appeared to influence the work reported in this paper.

Data availability

Data will be made available on request.

Acknowledgement

T Pandiyarajan gratefully acknowledges the Indian Institute of Information Technology Design and Manufacturing Kurnool for sanctioning Research Seed Money for financial assistance.

Appendix A. Supplementary material

Supplementary data to this article can be found online at https://doi.org/10.1016/j.inoche.2022.110383.

References

[1] H. Ohta, H. Hosono, Transparent oxide optoelectronics, Mater. Today (2004), https://doi.org/10.1016/S1369-7021(04)00288-3.

[2] E. Fortunato, D. Ginley, H. Hosono, D.C. Paine, Transparent Conducting Oxides for Photovoltaics, MRS Bull. (2007), https://doi.org/10.1557/mrs2007.29.

[3] S. Pal, N. Pal, A. Verma, J.P. Saini, Y.K. Prajapati, Analyzing the role of transparent conducting oxide in place of metals in SPR sensor for biomolecular detection in near infrared range, Results in Optics (2021), https://doi.org/10.1016/j.rio.2021.100078.

[4] P.C. Wang, L.H. Liu, D.A. Mengistie, K.H. Li, B.J. Wen, T.S. Liu, C.W. Chu, Transparent electrodes based on conducting polymers for display applications, Displays (2013), https://doi.org/10.1016/j.displa.2013.05.003.

[5] D. Yin, Z.Y. Chen, N.R. Jiang, Y.F. Liu, Y.G. Bi, X.L. Zhnag, W. Han, J. Feng, H.B. Sun, Highly transparent and flexible fabric-based organic light emitting devices for unnoticeable wearable displays, Org. Electron. (2020), https://doi.org/10.1016/j.orgel.2019.105494.

[6] N.N. Rosli, M.A. Ibrahim, N.A. Ludin, M.A.M. Teridi, K. Sopian, A review of graphene based transparent conducting films for use in solar photovoltaic applications, Renew. Sustain. Energy Rev. (2019), https://doi.org/10.1016/j.rser.2018.09.011.

[7] D.R. Cairns, R.P. Witte, D.K. Sparacin, S.M. Sachsman, D.C. Paine, G.P. Crawford, Strain-dependent electrical resistance of tin-doped indium oxide on polymer substrates, Appl. Phys. Lett. 10 (1063/1) (2000) 126052, https://doi.org/10.1063/1.126052.

[8] S.K. Park, J.I. Han, D.G. Moon, W.K. Kim, Mechanical Stability of Externally Deformed Indium–Tin–Oxide Films on Polymer Substrates, Jpn. J. Appl. Phys. (2003), https://doi.org/10.1143/JJAP.42.623.

[9] J. Li, S. Sathasivam, A. Taylor, C.J. Carmalt, I.P. Parkin, Single step route to highly transparent, conductive, and hazy aluminium doped zinc oxide films, RSC Adv. (2018), https://doi.org/10.1039/C8RA09338E.

[10] F. Yang, J. Song, X. Chen, X. Lu, J. Li, Q. Xue, B. Han, X. Meng, J. Li, Y. Wang, Ultrasonic spray pyrolysis-induced growth of highly transparent and conductive F Cl, Al, and Ga co-doped ZnO films, Solar Energy (2021), https://doi.org/10.1016/j.solener.2021.09.058.

[11] P.S. Huang, F. Qin, J.K. Lee, Role of the Interface between Ag and ZnO in the Electric Conductivity of Ag Nanoparticle-Embedded ZnO, ACS Appl. Mater. Interfaces (2020), https://doi.org/10.1021/acsami.9b17922.

[12] T. Grünleitner, A. Henning, M. Bissolo, A. Kleibert, C.A.F. Vaz, A.V. Stier, J.J. Finley, I.D. Sharp, Electronically Tunable Transparent Conductive Thin Films for Scalable Integration of 2D Materials with Passive 2D–3D Interfaces, Adv. Funct. Mater. (2022), https://doi.org/10.1002/adfm.202111343.

[13] Song Y, Fang W, Brenes R, Kong J. (2015) Challenges and opportunities for graphene as transparent conductors in optoelectronics, nanotoday 10.1016/j.nantod.2015.11.005.

[14] A.S. Mayorov, R.V. Gorbachev, S.V. Morozov, L. Britnell, R. Jalil, L.A. Ponomarenko, P. Blake, K.S. Novoselov, K. Watanabe, T. Taniguchi, Micrometer-scale ballistic transport in encapsulated graphene at room temperature, Nano Lett. (2011), https://doi.org/10.1021/nl200758b.

[15] A.A. Balandin, S. Ghosh, W. Bao, I. Calizo, D. Teweldebrhan, F. Miao, C.N. Lau, Superior thermal conductivity of single-layer graphene, Nano Lett (2008), https://doi.org/10.1021/nl0731872.

[16] Y.W. Sun, D.G. Papageorgiou, C.J. Humphreys, D.J. Dunstan, P. Puech, J.E. Proctor, C. Bousige, D. Machon, A. San-Miguel, Mechanical properties of graphene, Appl. Phys. Rev. DOI 10 (1063/5) (2021) 0040578.

[17] D.E. Sheehy, J. Schmalian, Optical transparency of graphene as determined by the fine-structure constant, Phys. Rev. B (2009), https://doi.org/10.1103/PhysRevB.80.193411.

[18] J. Wu, X. Shen, L. Jiang, K. Wang, K. Chen, Solvothermal synthesis and characterization of sandwich-like graphene/ZnO nanocomposites, Appl. Surf. Sci. (2010), https://doi.org/10.1016/j.apsusc.2009.11.034.

[19] Z. Li, P. Liu, G. Yun, K. Shi, X. Lv, K. Li, J. Xing, B. Yang, 3D (Three-dimensional) sandwich-structured of ZnO (zinc oxide)/rGO (reduced graphene oxide)/ZnO for high performance supercapacitors, Energy (2014), https://doi.org/10.1016/j.energy.2014.03.003.

[20] Teh S. J, Lai C. W, Abd. Hamid S. B. (2016) Novel layer-by-layer assembly of rGO-hybridised ZnO sandwich thin films for the improvement of photo-catalysed hydrogen production, J Ener Chem 10.1016/j.jechem.2016.01.009.

[21] I. Boukhoubza, M. Khenfouch, M. Achehboune, B.M. Mothudi, I. Zorkani, A. Jorio, Graphene oxide/ZnO nanorods/graphene oxide sandwich structure: The origins and mechanisms of photoluminescence, J. Alloys and Compd (2019), https://doi.org/10.1016/j.jallcom.2019.04.266.

[22] M. Ohyama, H. Kozuka, T. Yoko, Sol-gel preparation of ZnO films with extremely preferred orientation along (002) plane from zinc acetate solution, Thin Solid Films (1997), https://doi.org/10.1016/S0040-6090(97)00231-9.

[23] X. Jiao, Y. Qiu, L. Zhang, X. Zhang, Comparison of the characteristic properties of reduced graphene oxides synthesized from natural graphites with different graphitization degrees, RSC Adv. (2017), https://doi.org/10.1039/C7RA10809E.

[24] C. Suryanarayana, N.M. Grant, X-ray diffraction: a practical approach, Plenum Press, New York, 1998, p. 213.

[25] X.S. Wang, Z.C. Wu, J.F. Webb, Z.G. Liu, Ferroelectric and dielectric properties of Li-doped ZnO thin films prepared by pulsed laser deposition, Appl Phys A (2003), https://doi.org/10.1007/s00339-002-1497-2.

[26] Tu¨zemen E. S, Eker S, Kavak H, Esen R, (2009) Dependence of film thickness on the structural and optical properties of ZnO thin films, Applied Surface Science 10.1016/j.apsusc.2009.01.078.

[27] P. Liang, F. Wang, Z. A. Hu, Controlled synthesis of ordered sandwich $CuCo_2O_4$/reduced graphene oxide composites via layer-by-layer heteroassembly for high-performance supercapacitors, Chemical Engineering Journal 10.1016/j.cej.2018.06.021.

[28] O. Akhavan, R. Azimirad, S. Safa, Functionalized carbon nanotubes in ZnO thin films for photoinactivation of bacteria, Mater Chem Phys (2011), https://doi.org/10.1016/j.matchemphys.2011.07.030.

[29] C. Rodwihok, D. Wongratanaphisan, Y.L.T. Ngo, M. Khandelwal, S.H. Hur, J.S. Chung, Effect of GO Additive in ZnO/rGO Nanocomposites with Enhanced Photosensitivity and Photocatalytic Activity, Nanomaterials (2019), https://doi.org/10.3390/nano9101441.

[30] R. Paul, R.N. Gayen, S. Biswas, S.V. Bhat, R. Bhuni, Enhanced UV detection by transparent graphene oxide/ZnO composite thin films, RSC Adv. (2016), https://doi.org/10.1039/C6RA05039E.

[31] S. Alamdari, M.S. Ghamsari, H. Afarideh, A. Mohammadi, S. Geranmayeh, M.J. Tafreshia, M.H. Ehsani, M.H. Majlesarad, Preparation and characterization of GO-ZnO nanocomposite for UV detection application, Opt. Mater. (2019), https://doi.org/10.1016/j.optmat.2019.04.041.

[32] B. Lin, Z. Fu, Y. Jia, Green luminescent center in undoped zinc oxide films deposited on silicon substrates, Appl. Phys. Lett. (2001), https://doi.org/10.1063/1.1394173.

[33] P.S. Xu, Y.M. Sun, C.S. Shi, F.Q. Xu, H.B. Pan, The electronic structure and spectral properties of ZnO and its defects, Nucl. Inst. Methods Phys. Res. B (2003), https://doi.org/10.1016/S0168-583X(02)01425-8.

[34] Djuris˘ic A. B, Leung Y. H, (2006) Optical Properties of ZnO Nanostructures, small 10.1002/smll.200600134.

[35] Xiang Q, Yu J, Jaroniec M. (2011) Preparation and Enhanced Visible-Light Photocatalytic H_2-Production Activity of Graphene/C3N4 Composites, J. Phys. Chem. C 10.1021/jp200953k.

[36] S. Sarkar, D. Basak, One-step nano-engineering of dispersed Ag–ZnO nanoparticles' hybrid in reduced graphene oxide matrix and its superior photocatalytic property, CrstEngComm (2013), https://doi.org/10.1039/C3CE41043A.